Adaptive Cross Approximation for E-field-Guided Non-invasive Magnetic Brain Stimulation

Wang, Dezhi
Electrical and Computer Engineering
Purdue University
West Lafayette, USA
wang5355@purdue.edu

Dannhauer, Moritz
Psychiatry & Behavioral Sciences
Duke University
Durham, USA
moritz.dannhauer@duke.edu

Yucel, Abdulkadir C.
Electrical and Computer Engineering
NTU
Singapore, 639798
acyucel@ntu.edu.sg

Gomez, Luis J.
Electrical and Computer Engineering
Purdue University
West Lafayette, USA
ljgomez@purdue.edu

***Abstract*— Transcranial magnetic stimulation (TMS) is a non-invasive method that uses coils placed on the scalp to stimulate brain regions via magnetic induction. TMS is known to stimulate regions that are exposed to a large E-field magnitude. As a result, computational E-field dosimetry is increasingly being used to inform TMS administration. Existing methods for computational E-field dosimetry require substantial run-times that limit their applicability for many practical applications. We have developed a computational method based on adaptive cross approximations of matrices for fast computational E-field dosimetry of TMS. These methods will enable the development of improved TMS paradigms.**

Keywords—Adaptive Cross Approximation, brain stimulation, computational dosimetry

I. Introduction

Transcranial magnetic stimulation (TMS) is a non-invasive method for brain stimulation that uses a coil driven by low-frequency current pulses (>10kHz) to magnetically stimulate targeted brain regions. TMS is widely used for neuroscience research to study brain function and is FDA-approved for the treatment of depression and migraines. TMS has been shown to stimulate brain regions that are exposed to high E-fields. This has led to increased use of computational modeling for E-field dosimetry.

Computational methods for TMS E-field dosimetry use MRI-derived subject-specific volume conductor models and a TMS coil model to determine E-fields induced in the head when the coil is placed at a given position on the scalp. In principle, these methods could be iteratively applied to determine optimal coil placement on the scalp. For example, finding the coil position that maximizes E-field to the targeted brain region while avoiding another one. Furthermore, they could be used to incorporate inherent variabilities and uncertainties of the TMS setup into the simulation to predict the uncertainty of the TMS-induced E-field. An example is to determine E-field uncertainty resulting from limited precision and accuracy in coil placement. These and many other applications of TMS E-field solvers are currently impractical due to the long run-times of simulations, which are in the order of 10 of seconds. We present a method based on adaptive cross approximation (ACA) that after an initial setup stage of a few hours, it enables the generation of TMS coil position to E-field maps in seconds. These maps can then be used for TMS coil placement optimization and uncertainty quantification. (Note: For the range of frequencies of TMS pulses, quasi-stationary assumptions apply, as a result, temporal and spatial variations are separable and the temporal variation is suppressed in what follows.)

Research reported in this publication was supported by the National Institute of Mental Health under Award Number R00MH120046. The content of current research is solely the responsibility of the authors and does not necessarily represent the official views of the National Institutes of Health.

II. Methods

A. Discretization and matrix completion objective

The head is discretized into a tetrahedron mesh. In particular, the brain consists of a total of N_b tetrahedrons, and the scalp consists of N_t scalp boundary nodes. We discretize coil placements by assuming that the coil is always centered about a node on the scalp boundary, and all possible orientations are sampled one degree apart [Fig. 1]. The brain E-fields are assumed constant within each tetrahedron.

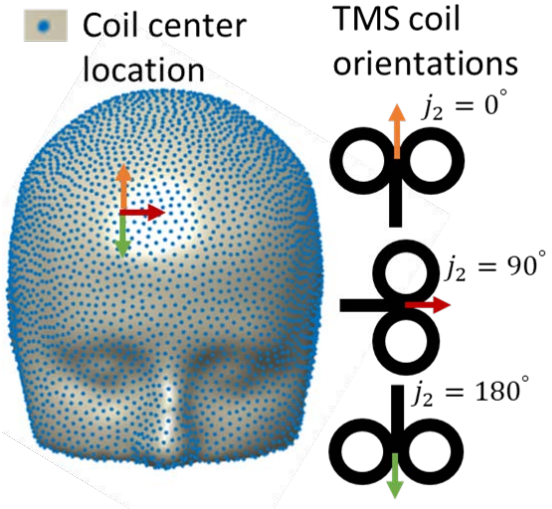

Fig. 1. The coil is assumed to always be placed tangent to the scalp and centered about one of the head mesh nodes depicted in blue. Furthermore, the orientation of the coil is indicated by an arrow as shown above.

Our goal is to obtain E-field values generated in every tetrahedron of a brain mesh region of interest (ROI) for all

possible coil placements. In other words, we would like to construct the matrix **A** of dimension $3N_b \times 360N_t$, where the entries are defined as

$$(\mathbf{A})_{3(i_1-1)+i_2,360(j_1-1)+j_2} = \begin{cases} \mathbf{E}_{j_1}^{(j_2)}(\mathbf{r}_{i_1}) \cdot \hat{\mathbf{x}} & i_2 = 1 \\ \mathbf{E}_{j_1}^{(j_2)}(\mathbf{r}_{i_1}) \cdot \hat{\mathbf{y}} & i_2 = 2. \\ \mathbf{E}_{j_1}^{(j_2)}(\mathbf{r}_{i_1}) \cdot \hat{\mathbf{z}} & i_2 = 3 \end{cases} \quad (1)$$

Here $i_1 = \{1,2,\dots,N_b\}$, $i_2 = \{1,2,3\}$, $j_1 = \{1,2,\dots,N_t\}$, $j_2 = \{1,2,\dots,360\}$ and $\mathbf{E}_{j_1}^{(j_2)}(\mathbf{r}_{i_1})$ is the E-field generated at the center of the i_1 th tetrahedron $\mathbf{r}_{i_1}$ assuming the coil is placed centered at the j_1 th node and oriented to point j_2 degrees clockwise from the back of the head as shown in Fig. 1.

The next subsection describes approaches for rapidly computing rows and columns of **A** enabling its generation using an interpolatory decomposition like the ACA described after the next subsection.

B. Determining $\boldsymbol{E}_{j_1}^{(j_2)}(\boldsymbol{r}_{i_1})$

The coil currents when the coil is placed at location j_1 and oriented along j_2 th orientation are denoted as $\mathbf{J}_{j_1}^{(j_2)}(\mathbf{r})$ and the corresponding E-field they generate in free-space is denoted as $\mathbf{E}_{\mathbf{inc}}{}_{j_1}^{(j_2)}(\mathbf{r})$. Quasi-stationary assumptions dictate that $\mathbf{E}_{j_1}^{(j_2)}(\mathbf{r}) = -\nabla\phi(\mathbf{r}) + \mathbf{E}_{\mathbf{inc}}{}_{j_1}^{(j_2)}(\mathbf{r})$, where $\nabla \cdot \sigma(\mathbf{r})\nabla\phi(\mathbf{r}) = \nabla \cdot \sigma(\mathbf{r})\mathbf{E}_{\mathbf{inc}}{}_{j_1}^{(j_2)}(\mathbf{r})$, the normal component of $\nabla\phi(\mathbf{r})$ is zero on the boundary and $\sigma(\mathbf{r})$ is the conductivity [1]. To determine $\nabla\phi(\mathbf{r})$, we use an in-house 1st order FEM method [1]. The above solution enables us to compute a column of the matrix **A** with the run-time equal to a single FEM solution.

To apply many interpolatory decompositions, like the ACA used here, we would like to compute the matrix's rows. Our previously developed auxiliary dipole method (ADM) is used for this purpose. ADM enables the computation of the average E-field generated in a prespecified ROI for all possible coil placements [2]. We use ADM to find the average E-field in the i_1 th tetrahedron along a direction $\hat{\mathbf{t}}$. We first define a source as $\mathbf{J}_{\mathbf{C}_{i_1}}^{(i_2)}(\mathbf{r}) = 1/V_{i_1}\,\hat{\mathbf{t}}$ on the i_1 th tetrahedron and zero elsewhere, where V_{i_1} is the volume of the i_1 th tetrahedron and $\hat{\mathbf{t}}$ is the principal direction corresponding to i_2. Second, we determine the E-fields that the auxiliary source generates outside the head $\mathbf{E}_{\mathbf{C}_{i_1}}^{(i_2)}(\mathbf{r})$. Reciprocity will dictate that the average E-field along $\hat{\mathbf{t}}$ will be

$$\mathbf{E}_{j_1}^{(j_2)}(\mathbf{r}_{i_1}) \cdot \hat{\mathbf{t}} = \int \mathbf{E}_{\mathbf{C}_{i_1}}^{(i_2)}(\mathbf{r}) \cdot \mathbf{J}_{j_1}^{(j_2)}(\mathbf{r})\mathrm{d}\mathbf{r}. \quad (2)$$

Equation (2) is rapidly evaluated using fast-multiple methods and an efficient quadrature rule described in [2]. For more detailed descriptions of both our FEM solver and ADM, the reader is referred to [1]-[2].

C. ACA

The previous section described a method for computing rows and columns of the matrix **A** enabling the use of ACA to approximate **A**. Details of the ACA can be found here [3]. Briefly, at the k[th] iteration the ACA algorithm constructs a k rank matrix $\widetilde{\mathbf{A}}^{(k)}$ from k linearly independent columns and rows of **A** that approximate **A** with error orthogonal to its row and column spaces. During each iteration, additional columns to be appended to the approximation are determined in a greedy way by using all previously computed rows and columns of **A** to infer the column and row that results will result in the largest correction.

III. Results

A. Sphere head model

As a first scenario, we consider a three-sphere head model as shown in Fig. 2(a). All of the admissible coil positions are shown in black and the 1 cm diameter ROI is shown by a red region. We considered two ROIs: one of 1 cm diameter [Fig.2(a)] and a 2 cm diameter ROI generated by growing the 1 cm diameter ROI. The relative L^2 norm error for an SVD compression, ACA compression, and predicted stop criterion as a function of rank is shown in Fig. 3. We observe that the SVD can achieve a 2% relative L^2-norm error with a rank 11 approximation for both ROI diameters of 1 cm and 2 cm. The ACA achieves a 2 % error using a rank 17 approximation for ROI diameter of 1 cm and a rank 25 approximation for ROI diameter of 2 cm. The ACA is able to achieve near optimal results without the necessity to compute the whole matrix. Furthermore, the red and black curves in Fig. 2 have some correspondence indicating that the ACA stop criterion is a good predictor of actual ACA accuracy enabling its use to determine if appropriate accuracy has been achieved.

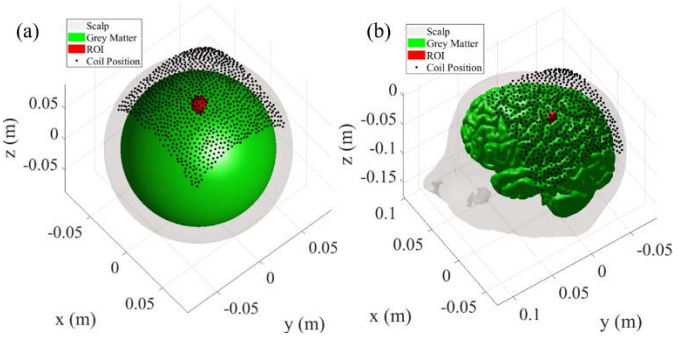

Fig. 2. Two different scenarios. (a) The three-sphere head model scenario and (b)an MRI-derived head model scenario.

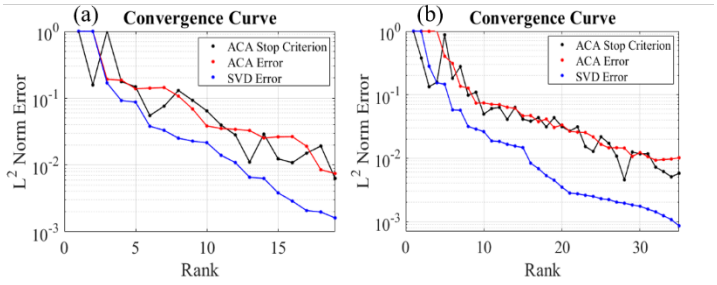

Fig. 3. Convergence curves for two different ROIs for the sphere head scenario. (a) The diameter of the ROI is 1 cm and (b) the diameter of the ROI is 2 cm.

B. *MRI-derived head model*

As a second scenario, we considered an MRI-derived head model as shown in Fig. 2(b) [4]. All of the admissible coil positions are shown in black and the 1 cm diameter cortical ROI is shown by the red region. We considered two ROIs: one of 1 cm diameter [Fig.2(b)] and a 2 cm diameter ROI generated by growing the 1 cm diameter ROI. The relative L^2 norm error for an SVD compression, ACA compression, and predicted stop criterion as a function of rank is shown in Fig. 4. We observe that the SVD can achieve a 2% relative L^2 norm error with a rank 7 approximation for ROI diameter of 1 cm and a rank 8 approximation for ROI diameter of 2 cm. The ACA achieves a 2 % error using a rank 12 approximation for ROI diameter of 1 cm and a rank 17 approximation for ROI diameter of 2 cm. The ACA results are consistent with those obtained for the sphere head model.

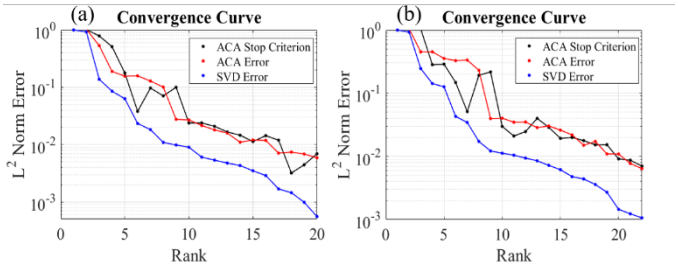

Fig. 4. Convergence curves for two different ROI sizes for the MRI-derived head scenario. (a) Diameter of the ROI is 1 cm; (b) Diameter of the ROI is 2 cm.

IV. Conclusion

ACA in conjunction with reciprocity enables the fast computation of coil location and orientation to cortical E-field mappings without the need to compute a matrix inverse and by just using the solution to a few sample coil locations and orientations. The use of such methods reduces the computational time of running E-field simulations significantly and can be used non-intrusively. TMS coil placement to E-field maps can be used for brain mapping [5], and a fast solver like the one presented here will enable the wide adoption of such methods.

V. References

[1] L. J. Gomez, M. Dannhauer, L. M. Koponen and A. Peterchev, "Conditions for numerically accurate TMS electric field simulation," *Brain Stimulation: Basic, Translational, and Clinical Research in Neuromodulation*, vol. 13, no. 1, pp. 157-166, 2020.

[2] L. J. Gomez, M. Dannhauer and A. Peterchev, " Fast computational optimization of TMS coil placement for individualized electric field targeting," *NeuroImage*, vol. 228, no. 3, pp. 1-13, 2021.

[3] K. Zhao, M. N. Vouvakis and J.-F. Lee, "The adaptive cross approximation algorithm for accelerated method of moments computations of EMC problems", *IEEE Trans. Electromagn. Comp.*, vol. 47, no. 4, pp. 763-773, 2005.

[4] A. Thielscher, A. Antunes and G. B. Saturnino, "Field modeling for transcranial magnetic stimulation: A useful tool to understand the physiological effects of TMS?," *2015 37th Annual International Conference of the IEEE Engineering in Medicine and Biology Society (EMBC)*, 2015, pp. 222-225.

[5] K. Weise, O. Numssen, A. Thielscher and G. Hartwigsen, and T. R. Knösche, " A novel approach to localize cortical TMS effects," *NeuroImage*, vol. 209, no. 1, pp. 1-17, 2020.